AGU PUBLICATIONS

Geochemistry, Geophysics, Geosystems

RESEARCH ARTICLE
10.1002/2016GC006286

Key Points:
- Base level friction, and friction velocity- and time-dependence all correlate
- Macroscopic fault friction for is controlled by grain-scale plastic deformation processes
- Real area of contact, activation energy, hardness, activation volume are important

Supporting Information:
- Supporting Information S1
- Table S1

Correspondence to:
M. J. Ikari,
mikari@marum.de

Citation:
Ikari, M. J., B. M. Carpenter, and C. Marone (2016), A microphysical interpretation of rate- and state-dependent friction for fault gouge, *Geochem. Geophys. Geosyst.*, *17*, 1660–1677, doi:10.1002/2016GC006286.

Received 1 FEB 2016
Accepted 6 APR 2016
Accepted article online 12 APR 2016
Published online 6 MAY 2016

© 2016. American Geophysical Union. All Rights Reserved.

A microphysical interpretation of rate- and state-dependent friction for fault gouge

Matt J. Ikari[1,2], Brett M. Carpenter[2,3], and Chris Marone[2]

[1]MARUM, Center for Marine Environmental Sciences, University of Bremen, D-28359, Bremen, Germany, [2]Department of Geosciences, Pennsylvania State University, University Park, Pennsylvania, USA, [3]School of Geology and Geophysics, University of Oklahoma, Norman, Oklahoma, USA

Abstract The evolution of fault strength during the seismic cycle plays a key role in the mode of fault slip, nature of earthquake stress drop, and earthquake nucleation. Laboratory-based rate- and state-dependent friction (RSF) laws can describe changes in fault strength during slip, but the connections between fault strength and the mechanisms that dictate the mode of failure, from aseismic creep to earthquake rupture, remain poorly understood. The empirical nature of RSF laws remains a drawback to their application in nature. Here we analyze an extensive data set of friction constitutive parameters with the goal of illuminating the microphysical processes controlling RSF. We document robust relationships between: (1) the initial value of sliding (or kinetic) friction, (2) RSF parameters, and (3) the time rates of frictional strengthening (aging). We derive a microphysical model based on asperity contact mechanics and show that these relationships are dictated by: (1) an activation energy that controls the rate of asperity growth by plastic creep, and (2) an inverse relationship between material hardness and the activation volume of plastic deformation. Collectively, our results illuminate the physics expressed by the RSF parameters, and which describe the absolute value of frictional strength and its dependence on time and slip rate. Moreover, we demonstrate that seismogenic fault behavior may be dictated by the interplay between grain properties and ambient conditions controlling the local shear strength of grain-scale asperity contacts.

1. Introduction

The evolution of fault strength during the seismic cycle plays a central role in determining earthquake source properties and the mode of fault slip. In the context of the seismic cycle, a simple requirement is that fault strength must recover during the interseismic period by an amount roughly equal to the earthquake stress drop. However, the underlying processes of fault restrengthening and frictional aging are poorly understood. Laboratory-based rate- and state-dependent friction (RSF) laws can describe fault restrengthening (aging) after stick-slip failure, but the empirical nature of those laws hinders their application to earthquake faulting. Moreover, RSF laws describe only the changes in friction in response to changing slip rate and do not address the absolute value of frictional strength or possible relationships between fault strength and stability of sliding.

In laboratory friction experiments designed to simulate fault slip and the seismic cycle, two types of tests are typically employed. In velocity-step tests, the shear strength of fault material is measured in response to sudden changes in the imposed shear displacement rate. These are most relevant to the earthquake nucleation process because a strength reduction upon an increase in slip rate is a requirement for frictional instability and dynamic earthquake rupture propagation [*Dieterich*, 1978, 1979, 1981, 1992; *Ruina*, 1983; *Rice and Ruina*, 1983; *Gu et al*., 1984; *Marone*, 1998a; *Scholz*, 2002]. Slide-hold-slide (SHS) tests measure the rate of frictional strengthening (aging), which is often called the rate of frictional healing in cases of strength recovery. These tests typically involve shearing at a constant rate, and then holding the driving rate stationary for a period of time before shear is resumed [e.g., *Dieterich*, 1972; *Beeler et al*., 1994; *Karner et al*., 1997; *Marone*, 1998b; *Karner and Marone*, 2001; *Nakatani and Scholz*, 2004a, 2004b; *Marone and Saffer*, 2015]. SHS tests are an approximate analogue for the seismic cycle in the sense that fault slip is followed by a period when the fault is locked or partially locked and creeping, during which elastic strain energy accumulates. A tectonic fault that experiences repeated earthquake rupture must exhibit two types of behavior: (1) slip or velocity weakening friction, such that instability can occur, and (2) the ability to regain shear strength after failure.

The prevailing constitutive laws used to describe velocity- and time-dependent variations of fault strength in the laboratory are known as rate- and state-friction (RSF) laws. The popularity of these laws is based not only on their ability to describe laboratory data, but also to simulate a wide range of fault behavior, including earthquake nucleation and rupture [e.g., *Tse and Rice*, 1986; *Cao and Aki*, 1986; *Tullis*, 1988; *Okubo*, 1989; *Dieterich*, 1992; *Rubin and Ampuero*, 2005; *Bizzarri*, 2011], afterslip [e.g., *Marone et al*., 1991; *Perfettini and Avouac*, 2004, 2007], and slow slip events [e.g., *Liu and Rice*, 2005; *Shibazaki and Shimamoto*, 2007; *Rubin*, 2008, 2011; *Skarbek et al*., 2012]. The full utility of these laws, however, depends on their ability to represent geologic processes operating on natural faults at an appropriate range of slip rates, time scales and length scales. Moreover, these laws are derived from empirical laboratory observations [*Dieterich*, 1972, 1978, 1979, 1981; *Ruina*, 1983], and the underlying physicochemical processes and deformation mechanisms are not well understood. This is one reason why extrapolation of laboratory results to in-situ conditions and tectonic environments is difficult.

Numerous studies have sought to better connect the RSF parameters with process-based models and geologic mechanisms [e.g., *Brechet and Estrin*, 1994; *Estrin and Bréchet*, 1996; *Rice et al*., 2001; *Sleep*, 2005, 2006; *Niemeijer and Spiers*, 2006, 2007; *Baumberger and Caroli*, 2006; *Boettcher et al*., 2007; *Beeler et al*., 2007; *Li et al*., 2011; *King and Marone*, 2012; *den Hartog and Spiers*, 2013, 2014; *Bar-Sinai et al*., 2014]. Of particular interest is the relationship between macroscopic fault strength (here quantified as a base value, steady-state friction coefficient) and its dependence on time and slip rate described by RSF. The latter dictate fault slip stability, while the former determines heat production and the energy budget of faulting. The basic theory of earthquake mechanics suggests that fault stability and stress drop are independent of fault strength [*Brace and Byerlee*, 1966; *Byerlee*, 1970; *Tullis*, 1988]. However, this has been called into question by recent works [*Beeler*, 2007; *Ikari et al*., 2011a], and earlier laboratory studies have suggested that weak materials tend to suppress frictional instability [e.g., *Brace*, 1972; *Shimamoto and Logan*, 1981], which would suggest a relationship between base friction and RSF properties.

The purpose of this paper is twofold. First, we analyze the results of frictional shearing experiments described in *Carpenter et al*. [2016]. In addition, we use those data, and existing studies, to investigate the relationships between base friction and RSF parameters. We derive a micromechanical model and strive to illuminate the physical basis for RSF laws and unstable fault slip. *Carpenter et al*. [2016] describe measurements of time-dependent frictional strengthening from SHS tests to investigate fault strength recovery and frictional aging. By integrating the results of these tests with measurements of RSF parameters from velocity-step tests, we explore the underlying microphysical mechanisms that determine friction, focusing on the relationship between velocity dependence, time dependence, and the role of the absolute value of fault strength for a wide range of fault materials including natural fault gouge and synthetic gouges derived from mineral standards.

2. Constitutive Framework for Laboratory Friction Measurements

2.1. Experimental Methods

We analyze here results of laboratory friction experiments first reported in *Carpenter et al*. [2016], for which two groups of fault gouges were tested: (1) natural fault gouges from subduction, strike-slip, and normal fault zone settings, and (2) synthetic gouges, either ground from commonly occurring rocks or obtained as commercial powders (Table 1). During these experiments both slide-hold-slide and velocity step tests were conducted (Figure 1); results of the SHS tests are described in *Carpenter et al*. [2016], while results of velocity step tests are reported here. The experiments were conducted in a biaxial testing apparatus using the double-direct shear geometry. Ambient relative humidity (100%), temperature (27°C), and normal stress (20 MPa during measurements) were maintained constant in all experiments. Samples were sheared at a constant velocity of 11 μm/s until a shear strain of ~15, after which residual steady state shear stress was measured. This experimentally measured shear strength τ depends on the coefficient of friction μ, the applied normal stress σ_n, and the cohesive strength c [*Handin*, 1969]:

$$\tau = \mu\sigma_n + c. \quad (1)$$

In this paper we use μ to quantify fault strength, rather than the shear strength τ which is in most cases highly dependent on normal stress, and thus depth. Although it has been demonstrated that cohesive

Table 1. Results of Friction Measurements[a]

Gouge	Sample	Wt% Water[a]	μ_o	β (decade^{-1})	a-b	a	b_1+b_2
Talc	synthetic gouge	1.0	0.22	0.0005	0.0030	0.0027	−0.0003
			0.21		0.0028	0.0033	0.0005
Montmorillonite	synthetic gouge	16.3	0.11	0.0018	0.0047	0.0034	−0.0014
			0.08		0.0060	0.0038	−0.0023
Kaolinite	synthetic gouge	2.5	0.28	0.0031	0.0027	0.0045	0.0018
			0.26		0.0037	0.0054	0.0017
Rochester Shale	synthetic gouge	3.7	0.42	0.0011	0.0028	0.0034	0.0006
			0.40		0.0027	0.0035	0.0008
Biotite	synthetic gouge	0.4	0.22	0.0014	0.0037	0.0057	0.0020
			0.19		0.0039	0.0072	0.0033
Westerly Granite	synthetic gouge	0.3	0.57	0.0069	−0.0005	0.0076	0.0081
			0.55		0.0001	0.0088	0.0087
Andesine	synthetic gouge	0.0	0.60	0.0068	−0.0004	0.0067	0.0071
			0.60		0.0007	0.0073	0.0066
Quartz sand	synthetic gouge	0.9	0.61	0.0064	−0.0010	0.0074	0.0084
			0.60		−0.0017	0.0075	0.0092
Calaveras fault	fault outcrop	1.0	0.62	0.0073	−0.0001	0.0087	0.0088
			0.61		−0.0001	0.0081	0.0076
San Andreas fault	SAFOD core G44	10.4	0.18	0.0010	0.0009	0.0025	0.0016
			0.18		0.0008	0.0023	0.0014
Nankai Decollement	ODP Leg 190 1174B-72R-1	5.8	0.40	0.0058	−0.0014	0.0035	0.0048
			0.32		0.0003	0.0045	0.0042
Alpine Fault	GC09-4 PSS	4.8	0.56	0.0118	−0.0007	0.0090	0.0096
			0.48		0.0015	0.0096	0.0082
Kodiak Ghost Rocks	SPP-06	1.0	0.58	0.0067	0.0004	0.0072	0.0068
			0.60		0.0023	0.0070	0.0047
San Gregorio fault	"A" fault gouge core	4.6	0.58	0.0079	0.0007	0.0089	0.0083
			0.52		0.0010	0.0080	0.0071
Zuccale fault	L3	5.9	0.29	0.0083	0.0027	0.0080	0.0053
			0.25		0.0019	0.0089	0.0070
Scheggia Thrust	hanging wall cataclasite	1.8	0.67	0.0105	−0.0036	0.0077	0.0112
			0.59		−0.0016	0.0076	0.0092
Costa Rica Decollement	ODP Leg 205 1255-2R-CC	6.0	0.56	0.0077	−0.0005	0.0046	0.0051
			0.47		0.0003	0.0058	0.0054

[a]Adsorbed water removed by post-experiment oven drying at 105°C.

strength can exist during sliding when clays are present [*Ikari and Kopf*, 2011], it is common in many friction studies to neglect c and compute $\mu = \tau/\sigma_n$, where μ is now the coefficient of sliding friction. We follow this convention, because our disaggregated samples, and the low pressure and temperature conditions employed, make these experiments directly applicable to brittle-frictional deformation of incohesive fault gouge [e.g., *Sibson*, 1977; *Woodcock and Mort*, 2008]. Therefore, we assume that our gouges deform purely

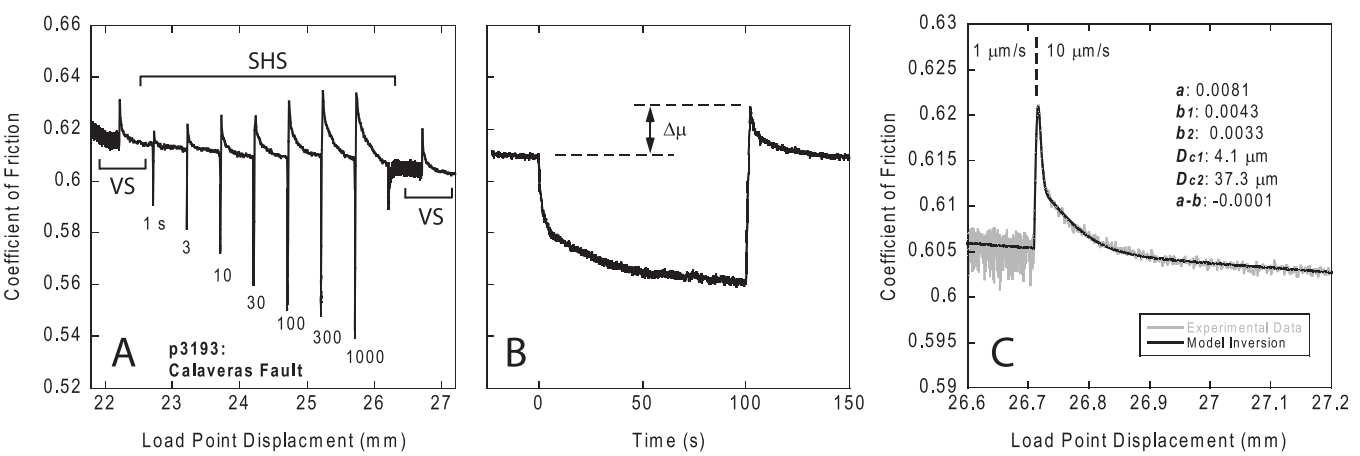

Figure 1. Friction data for gouge from the Calaveras fault zone, California. (a) Raw data for two velocity steps (VS) and a series of slide-hold-slide (SHS) tests with hold times from 1 to 1000 s. (b) Time series of friction data during a slide-hold-slide test showing the increase in "static" friction $\Delta\mu$. (c) Friction data for the second velocity step test in Figure 1a overlain by a RSF model with parameters as given. A two state variable friction response is seen.

by frictional mechanisms so that all changes in shear strength are due to changes in friction, μ. However, we note that this may not be the case in systems under hydrothermal conditions and higher temperature regimes, which are not addressed by these experiments.

2.2. Rate- and State-Friction

Velocity-stepping tests are a standard approach to determining RSF parameters, where the frictional response to a velocity step is described by the RSF relations:

$$\mu=\mu_o+a\ln\left(\frac{V}{V_o}\right)+b_1\ln\left(\frac{V_o\theta_1}{D_{c1}}\right)+b_2\ln\left(\frac{V_o\theta_2}{D_{c2}}\right) \tag{2}$$

$$\frac{d\theta_i}{dt}=1-\frac{V\theta_i}{D_{ci}},\ i=1,2 \tag{3}$$

where a, b_1 and b_2 are dimensionless parameters, θ_1 and θ_2 are state variables (units of time), and D_{c1} and D_{c2} are critical slip distances over which friction evolves to a new steady state value [*Dieterich*, 1979, 1981; *Ruina*, 1983]. The second term on the right hand side of equation (2) is known as the "direct effect", and the subsequent terms define the "evolution effect." Although we nominally employ the two-state variable law, we define $b=b_1+b_2$ and $\theta=\theta_1+\theta_2$; according to the convention that if data are well described by a single state variable then $D_{c1}=D_{c2}$ and we take $b_2=0$. Equation (3) describes the evolution of the state variable θ and is known as the "Dieterich" or "slowness" law, which has the property that friction can change as a function of time even in the limiting case of zero slip velocity [*Dieterich*, 1981; *Beeler et al*., 1994]. Recent work shows that an alternative law [*Ruina*, 1983] better describes frictional state evolution in some cases [*Bayart et al*., 2006; *Bhattacharya et al*., 2015], however other studies show that the value of $a-b$ is unaffected by the choice of evolution law [e.g., *Rathbun and Marone*, 2010] and we use here results of the Dieterich law interpretation.

For steady state frictional sliding, equations (2) and (3) reduce to:

$$a-b=\frac{\Delta\mu_{ss}}{\Delta\ln(V)} \tag{4}$$

where $\Delta\mu_{ss}$ is the new steady state friction value following the velocity step. The velocity-dependent friction parameter $a-b$ is critical for evaluating the seismogenic potential of faults [e.g., *Rice and Ruina*, 1983] because the nucleation of unstable slip and earthquake rupture requires velocity-weakening friction ($a-b<0$), as well as certain elastic conditions in the fault surroundings [e.g., *Gu et al*., 1984]. Although $a-b$ may be calculated by directly measuring the change in friction after the velocity step (equation (4)), the individual RSF parameters a, b_1, b_2, D_{c1} and D_{c2} must be determined by accounting for elastic interaction with the testing machine [e.g., *Tullis and Weeks*, 1986; *Reinen and Weeks*, 1993; *Marone*, 1998a]. This requires an expression for the system stiffness k (units of friction/displacement):

$$\frac{d\mu}{dt}=k(V_{lp}-V) \tag{5}$$

where $(V_{lp}-V)$ is the difference between fault slip velocity V and the remotely recorded load point velocity V_{lp}, and k is the stiffness of the testing machine, which includes the forcing blocks and support structure, and the fault zone of finite width. In the laboratory, system stiffness k includes the combined effects of the apparatus and sample [e.g., *Leeman et al*., 2015], although in our tests this is mostly due to apparatus stiffness. Inversion of friction data to obtain the RSF parameters involves solving equations (2), (3), and (5) simultaneously using an iterative, least-squares method [e.g., *Reinen and Weeks*, 1993; *Blanpied et al*., 1998]. Figure 1c shows an example of a comparison between the experimental data and the model. Our modeling procedure also allows the removal of long-term slip-dependent friction trends, in order to avoid biasing and more accurately determine the friction velocity dependence [e.g., *Blanpied et al*., 1998]. Standard deviations for the modeled parameters are also calculated, and are shown as error bars in Figure 2 (see also supporting information).

2.3. Frictional Healing

Carpenter et al. [2016] report results from slide-hold-slide (SHS) tests, during which samples are sheared at a given velocity and slip distance (typical values are 10 μm/s and 500 μm) and then loading is paused for a

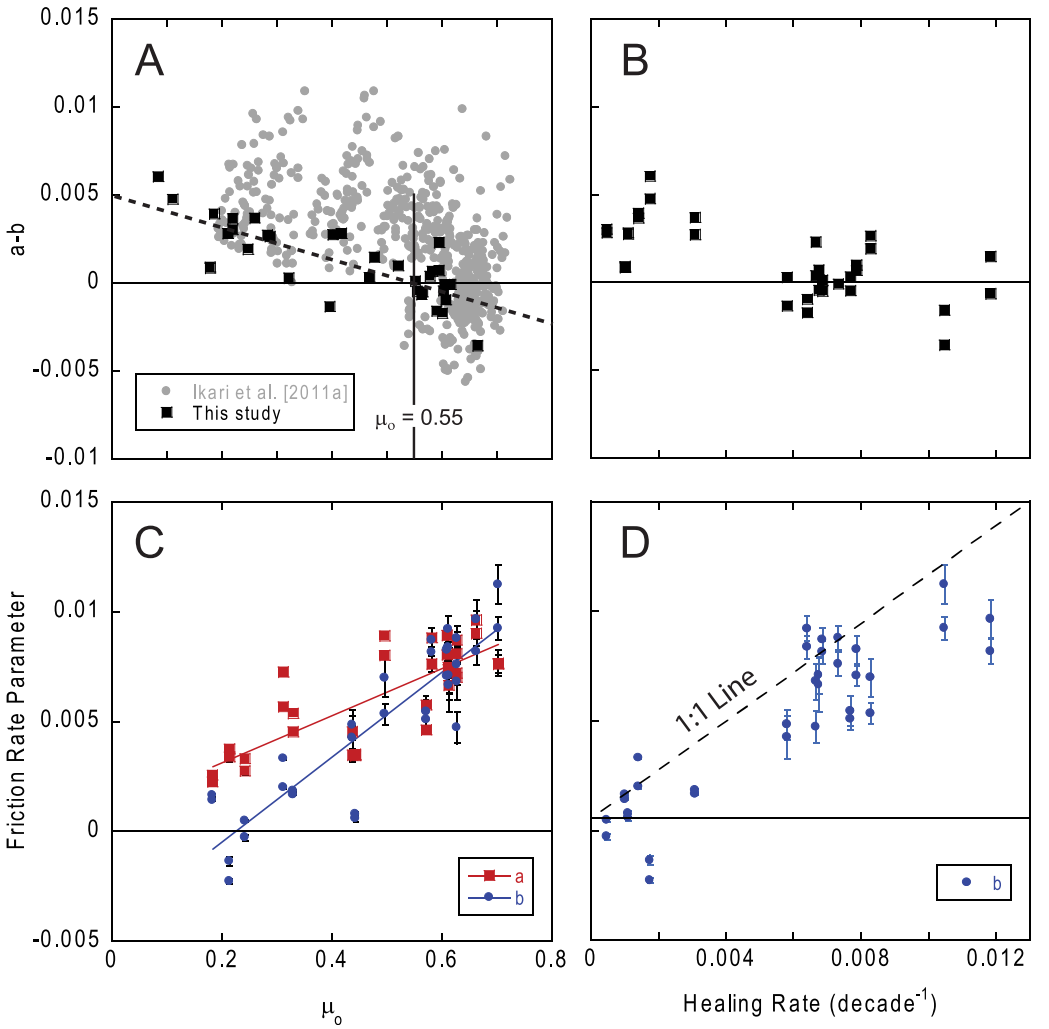

Figure 2. Compilation of RSF parameters from this study, and frictional healing rate β from *Carpenter et al.* [2016]. (a) The friction velocity parameter $a-b$ as a function of the initial coefficient of sliding friction μ_o, comparing results of this study with *Ikari et al.* [2011a]. Dashed line shows best-fit linear relation, with a crossover from velocity strengthening to velocity weakening at $\mu_o = 0.55$. (b) Friction rate parameter $a-b$ as a function of β. (c) Parameters a and b as functions of μ_o. Note that these data confirm the trend seen in Figure 2a: that is $da/d\mu_o < db/d\mu_o$. (d) State evolution parameter b as a function of the frictional healing rate β. The 1:1 line is shown for reference.

duration t_h (the "hold time") from 1 to 1000 s (Figure 1). During the "hold" portion of the SHS test, the driving velocity of the apparatus is held at $V_{lp} = 0$, and "static" friction increases ($\Delta\mu$) as a function of hold time are measured as the difference between the steady-state friction value immediately preceding the hold, and the peak in friction following reshear [e.g., *Rabinowicz*, 1956; *Dieterich*, 1972; *Beeler et al.*, 1994; *Marone and Saffer*, 2015]. The time rate of frictional strengthening β (decade^{-1}) is described as:

$$\Delta\mu = \beta\Delta \log t_h \tag{6}$$

[*Dieterich*, 1972; *Marone*, 1998b]. Also sometimes referred to as the frictional healing rate, β can be used as a proxy for interseismic strength recovery.

3. Empirical Relationships Between Friction Parameters

In a previous study, *Ikari et al.* [2011a] showed that $a-b$ has an inverse relationship with the steady-state coefficient of sliding friction μ_o. We expand their database by adding results from experiments performed by, but not presented in, *Carpenter et al.* [2016]. Negative values of $a-b$ occur primarily for materials with $\mu_o > \sim 0.55$ (Figure 2). These results are consistent with those of *Ikari et al.* [2011a], who showed that velocity

strengthening occurs for a wide range of fault gouges with $\mu < \sim 0.5$, and with an earlier model by *Beeler* [2007a]. The data of Figure 2 provide a clear, more precise view of the dependence of $a-b$ on sliding friction. This is because the earlier data [*Ikari et al*., 2011a] include measurements conducted over a wide range of shear strain (up to $\gamma = \sim 100$), whereas the data of *Carpenter et al*. [2016] were collected for a narrow range of shear strains near $\gamma = \sim 15$ to eliminate the commonly observed variation of RSF parameters with net displacement [*Dieterich*, 1981; *Beeler et al*., 1996; *Scruggs and Tullis*, 1998; *Mair and Marone*, 1999; *Richardson and Marone*, 1999; *Ikari et al*., 2011a].

Our data also show that both friction parameters a and b vary systematically with the coefficient of sliding friction μ_o (Figure 2). RSF parameter b increases more strongly with μ_o than does a, which results in the negative dependence of $a-b$ on μ_o. In some cases negative values of b are observed, which guarantees velocity-strengthening behavior [*Saffer and Marone*, 2003; *Ikari et al*., 2009, 2011b; *Carpenter et al*., 2012]. The observations of negative b are robust, and not an artifact of testing apparatus stiffness [*Sone et al*., 2012], however the exact cause of negative values of b is still debated.

We find that the parameters b and β lie near the 1:1 line (Figure 2). This confirms expectations from early experimental work on frictional aging [e.g., *Dieterich*, 1972, 1978, 1979, 1981] and predictions of RSF laws (for a recent summary, see *Marone and Saffer* [2015]). This can be understood by noting that for a SHS test where the pre and posthold velocities are equal, the healing parameter $\Delta\mu$ is measured when $V = V_o$; hence, the second term on the right hand side of equation (2) is zero and $\Delta\mu = b\ln(V_o\theta/D_c)$, where b, θ, and D_c indicate the parameters for one or two state variables as necessary. As V approaches zero, $d\theta/dt$ approaches 1 (equation (3)) and the state variable θ can be replaced by t_h. Thus, $\Delta\mu \approx b\ln(t_h)$, so that b describes a logarithmic dependence of friction on time which is functionally equivalent to the healing rate β determined from SHS tests (but note that b scales a natural logarithm in time, whereas β scales a $\log_{10}$ dependence in time) [*Beeler et al*., 1994; *Marone*, 1998b]. The correlation we observe between b and β shows that the healing rate β also depends positively on μ_o, and furthermore that $a-b$ has an inverse relationship with β (Figure 2).

4. Microphysical Model for Fault Gouge Friction

Most existing analyses of fault gouge friction with RSF assume that the coefficient of sliding friction μ_o is independent of the rate parameters a and b. This is implicit in the form of the RSF law, which is written in terms of a reference friction value with separate terms for the direct effect and evolution effect [e.g., *Dieterich*, 1979, 1981; *Ruina*, 1983; *Tullis*, 1988]. Early studies of RSF properties of fault gouge showed that friction rate dependence, $a-b$, varied with dilatancy rate [*Marone et al*., 1990], and recent process-based friction models have incorporated that relationship [e.g., *Niemeijer* and *Spiers*, 2007]. *Beeler* [2007a] reviewed a number of studies and suggested that the stability of frictional slip is related to dilatancy, with stronger materials tending to be more dilatant, thus providing a direct link between fault strength and stability. However, those data sets are sparse for weak materials. In a study considering data from several fault gouges, spanning a wide range of sliding friction values, *Ikari et al*. [2011a] found that velocity-weakening behavior was absent for gouges weaker than $\mu = \sim 0.5$, in support of *Beeler*'s [2007] argument.

A number of studies indicate that deformation of asperity contacts determines the frictional properties of rock [e.g., *Engelder and Scholz*, 1976; *Dieterich and Conrad*, 1984; *Logan and Teufel*, 1986; *Wang and Scholz*, 1994; *Goldsby et al*., 2004]. Early tribology works also showed that the size and quality of frictional contact junctions dictate the evolution of shear strength with contact time and slip [*Bowden and Tabor*, 1939, 1966; *Rabinowicz*, 1951, 1956; *Brockley and Davis*, 1968]. Additional work shows that the size of "real areas of contact" defined by individual asperities increases via plastic creep, as indicated by direct observation of contact area growth in quartz, calcite, glass, and acrylic [*Dieterich and Kilgore*, 1994, 1996] and from indentation tests [*Scholz and Engelder*, 1976; *Friedman and Higgs*, 1981; *Evans*, 1984; *Masuda et al*., 2000; *Goldsby et al*., 2004; *Zhang and Spiers*, 2005]. These studies show that creep at highly stressed contact junctions is significant, even at room temperature.

We use the laboratory results of *Carpenter et al*. [2016] to inform a microphysical model of plastic deformation at grain-scale asperity contacts based on previous results by several researchers [e.g., *Brechet and Estrin*, 1994; *Heslot et al*., 1994; *Estrin and Bréchet*, 1996; *Rice et al*., 2001; *Sleep*, 2005; *Baumberger and Caroli*, 2006; *Beeler et al*., 2007b; *Bar-Sinai et al*., 2014]. As a starting assumption, we posit that a correlation between fault

strength and slip stability can be reconciled by a microphysical model for RSF, where the RSF parameters a and b represent micromechanical processes and are not simply empirical constants. As an important caveat, we note that the correlations we observe between the parameters a, b and μ_o may arise from additional interdependencies and/or other factors that are not typically controlled in friction experiments.

From Amonton's Law, the coefficient of friction can be defined as the ratio of the shear traction F_S required for slip and the normal force F_N. For a nominal contact area A, these forces define the macroscopic shear (τ) and normal (σ_n) stresses, which are the sum of local stresses on real areas of contact A_c:

$$\mu = \frac{F_S}{F_N} = \frac{\tau A}{\sigma_n A} = \frac{\tau_c A_c}{\sigma_c A_c} \tag{7}$$

where τ_c and σ_c are the local shear and normal stress at the contacts. Fully plastic deformation at contact junctions occurs when the local normal stress approaches a limit defined by the material hardness H, (i.e., when $\sigma_c \approx H$) [*Bowden and Tabor*, 1966; *Dieterich and Kilgore*, 1994; *Nakatani and Scholz*, 2004b]. At this point the macroscopic frictional strength is controlled by fluctuations in A_c, which for many materials grows logarithmically with contact time [e.g., *Dieterich and Kilgore*, 1994, 1996]:

$$A_c = A_{c,o} + B \log (t/t_o) \tag{8}$$

where $A_{c,o}$ is the elastic real area of contact at the onset of plastic deformation, B is the time-dependent rate of increase in A_c, and t_o is a "cutoff time," or minimum amount of time necessary for nonnegligible increase in A_c. From experiments on quartz, t_o has been estimated to be ~1 s [e.g., *Marone*, 1998b; *Nakatani and Scholz*, 2004a], but for gouges with a significant component of clay minerals it may be closer to ~3–10 s [*Ikari et al.*, 2012]. The parameter B in equation (8) is calculated in a similar manner to β, but measures time-dependent changes in area rather than friction [*Dieterich and Kilgore*, 1994; *Bar-Sinai et al.*, 2014].

Replacing the local normal contact stress σ_c in equation (7) with the material hardness H, the initial contact area at the onset of plastic deformation becomes:

$$A_{c,o} = \frac{\sigma_n A}{H}, \tag{9}$$

and the time-dependent growth in contact area A_c is:

$$A_c = \frac{\sigma_n A}{H} + B \log (t/t_o). \tag{10}$$

Following *Rice et al.* [2001], the slip rate during sliding at contact junctions is described by an Arrhenius relationship:

$$V = V_o e^{\frac{-E}{\kappa T}} \tag{11}$$

where κ is the Boltzmann constant and T is the temperature, and E can be further decomposed to:

$$E = E_o - \tau_c \Omega \tag{12}$$

where E_o is the activation energy and Ω is the activation volume for the plastic strain accommodation mechanism. Combining equations (11) and (12) yields an expression for the local asperity contact shear strength τ_c:

$$\tau_c = \frac{E_o}{\Omega} + \frac{\kappa T}{\Omega} \ln \left(\frac{V}{V_o} \right). \tag{13}$$

The macroscopic shear force is the sum of the shear forces on the real areas of contact so that $\tau A = \tau_c A_c$ (equation (7)); therefore equations (10) and (13) can be combined to yield an expression for τ:

$$\tau = \frac{E_o \sigma_n}{H\Omega} + \frac{\kappa T \sigma_n}{H\Omega} \ln \left(\frac{V}{V_o} \right) + \frac{E_o B}{\Omega A} \log \left(\frac{t}{t_o} \right) + \frac{\kappa T B}{\Omega A} \ln \left(\frac{V}{V_o} \right) \log \left(\frac{t}{t_o} \right). \tag{14}$$

If we then incorporate the relations $\tau = \mu\sigma_n$, $t = \theta$, $t_o = D_c/V_o$, consider constant normal force so that $\sigma_n A = HA_c$, and convert the base 10 logarithm to natural log, we have:

$$\mu = \frac{E_o}{H\Omega} + \frac{\kappa T}{H\Omega}\ln\left(\frac{V}{V_o}\right) + \frac{E_o B}{2.3H\Omega A_c}\ln\left(\frac{V_o\theta}{D_c}\right) + \frac{\kappa TB}{2.3H\Omega A_c}\ln\left(\frac{V}{V_o}\right)\ln\left(\frac{V_o\theta}{D_c}\right). \quad (15)$$

This can be recognized as the empirical RSF equation (equation (2)) with:

$$\mu_o = \frac{E_o}{H\Omega}, \quad (16)$$

$$a = \frac{\kappa T}{H\Omega}, \quad (17)$$

and:

$$b = \frac{E_o B}{2.3H\Omega A_c} + \frac{\kappa TB}{2.3H\Omega A_c}\ln\left(\frac{V}{V_o}\right). \quad (18)$$

Using the relation for a (equation (17)), the evolution parameter b (equation (18)) can be written as:

$$b = \frac{E_o B}{2.3H\Omega A_c} + \frac{B}{2.3A_c}a\ln\left(\frac{V}{V_o}\right). \quad (19)$$

The contribution to b from the second term can be evaluated by comparing values of $a\ln(V/V_o)$ to $E_o/H\Omega$ by substituting equation (16) into equation (19) and using our experimentally measured values of a and μ_o. Doing so, we find that the second term on the right side of equation (19) represents $< 5\%$ of the total value of b and can therefore be neglected.

Substituting equation (16) into equation (17) and the simplified equation (19) reveals:

$$a = \frac{\mu_o \kappa T}{E_o}, \quad (20)$$

and:

$$b = \frac{\mu_o B}{2.3A_c}, \quad (21)$$

which is confirmed by our experimental data showing that both a and b depend positively on the base friction coefficient (Figure 2). Frictional slip instability requires $a - b < 0$, which requires $b/a > 1$, therefore we evaluate the ratio b/a by dividing equation (21) by equation (20):

$$\frac{b}{a} = \frac{E_o B}{2.3\kappa TA_c}. \quad (22)$$

Equation (22) indicates that at constant temperature, the rate dependence of friction (here given as b/a) can be described in terms of two parameters: the activation energy E_o and the rate of contact area growth B/A_c.

5. Evaluation of Model Predictions

5.1. Comparison With Previous Data

Using this model formulation, we find that the values of E_o range from 1.8 to 5.2 $\times$ 10^{-19} J and B/A_c ranges from -0.024 to 0.037. These E_o values are consistent with previous works which report E_o of $\sim$0.5 to 3.7 $\times$ 10^{-19} J for a range of materials including quartz, quartzite, calcite, granite, dolerite, halite, shale, muscovite and biotite [*Atkinson*, 1984; *Wawersik and Zeuch*, 1986; *Lockner*, 1993; *Kronenberg et al*., 1990; *Ibanez and Kronenberg*, 1993; *Mares and Kronenberg*, 1993; *Hirth et al*., 2001]. Fewer results have been reported for B/A_c. We note that the values determined from equation (21) match those of *Goldsby et al*. [2004] who report B/A_c $\sim$0.03 for quartz, but are somewhat lower than the $\sim$0.06 for glass reported by *Dieterich and Kilgore* [1994]. We observe some negative values of B/A_c, which are a consequence of negative measured values of b; nominally this suggests that contact area is decreasing with hold time, which may be explained by degradation of the contact quality [e.g., *Tullis*, 1988; *Li et al*., 2011] or creep driven by shear rather than normal traction [*Sleep*, 2005]. However, due to the uncertainty surrounding the physical origin of negative values of b, full investigation of the origin of this phenomenon is beyond the scope of the present work.

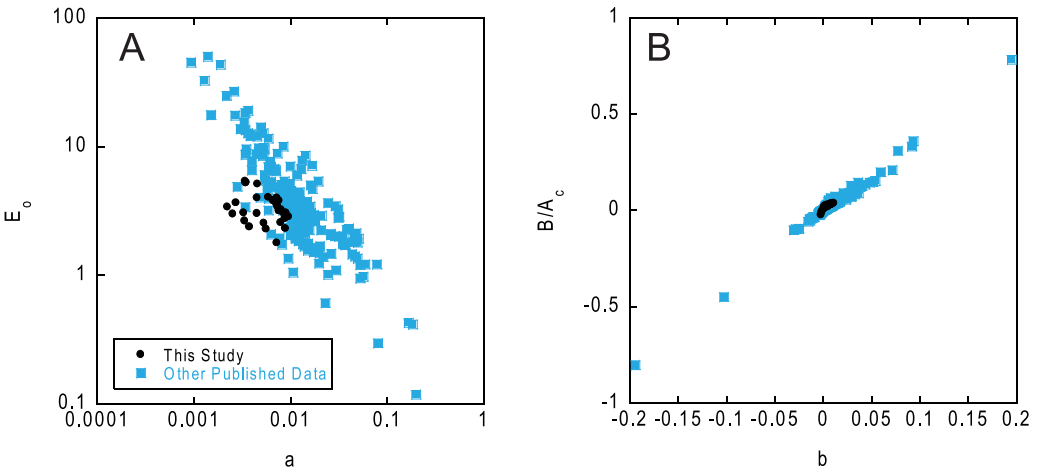

Figure 3. (a) Activation energy E_o as a function of the friction parameter a, and (b) normalized rate of change of the real area of contact B/A_c as a function of the rate-dependent friction parameter b. Our data (black circles) are compared with values calculated from previous works (blue squares) [*Weeks and Tullis*, 1985; *Chester*, 1994; *Reinen et al*., 1994; *Blanpied et al*., 1998; *Boettcher et al*., 2007; *den Hartog et al*., 2012; *Lu and He*, 2014; *Niemeijer and Collettini*, 2014; *Niemeijer and Vissers*, 2014]. Note that the data define a clear negative correlation between E_o and a (Figure 3a) and a clear positive correlation between the ratio B/A_c and the parameter b.

The model predicts specific relationships between RSF parameters, base friction, and plastic deformation parameters. In particular, with known values of temperature and the Boltzmann constant, equations (17), (20), and (21) predict that, respectively, a correlates inversely with E_o, and b correlates directly with B/A_c. We test these predicted relationships using our data and existing studies where friction parameters were determined for known temperatures. These data cover a wide range of conditions, with pressures up to 400 MPa and temperatures up to 1000°C. The materials include quartz [*Chester*, 1994], olivine [*Boettcher et al*., 2007], biotite [*Lu and He*, 2014], serpentine [*Reinen et al*., 1994], dolomite [*Weeks and Tullis*, 1985], Rochester shale [*den Hartog et al*., 2012], the Alhama de Murcia fault, Spain [*Niemeijer and Vissers*, 2014], the Zuccale fault, Italy [*Niemeijer and Collettini*, 2014], and Westerly granite [*Blanpied et al*., 1998].

There is a clear inverse (logarithmic) relationship between a and E_o and a direct (linear) relationship between b and B/A_c, as predicted by the theory (Figure 3). Data from our study match the trend of b as a function of B/A_c defined by existing studies and appear to also match the trend of a as a function of E_o, although there is quite a bit of scatter. Our room temperature data best match the low a and low E_o data, suggesting that higher temperatures are associated with both higher a and higher E_o. A positive correlation between b/a with E_o, as indicated by equation (22), is obscured by data scatter, although our data do show a positive trend (Figure 4). However, a positive trend between b/a and B/A_c is quite clear for both our data and literature-derived values. Moreover, most data appear to follow a consistent trend. Two exceptions are data for dolomite [*Weeks and Tullis*, 1985], and Westerly granite [*Blanpied et al*., 1998], but we note that the granite data also exhibit a positive relationship between b/a and B/A_c, with a lower slope.

As an additional consideration, the velocity-dependence of friction may also be controlled by the hardness H and the activation volume Ω. This can be seen by using equation (16) to substitute for E_o:

$$\frac{b}{a} = \frac{\mu_o H \Omega B}{2.3 \kappa T A_c}. \tag{23}$$

This indicates that the ratio b/a should be positively related to the hardness H and the activation volume Ω. Although the material hardness appears as a common feature of micromechanical tribology models, previous studies have not addressed a functional relationship between the measured frictional parameters and hardness (or activation volume) [*Brechet and Estrin*, 1994; *Heslot et al*., 1994; *Estrin and Bréchet*, 1996; *Baumberger*, 1997; *Baumberger et al*., 1999; *Persson*, 1999; *Rice et al*., 2001; *Nakatani and Scholz*, 2004b; *Sleep*, 2005; *Baumberger and Caroli*, 2006]. These studies, whose model derivations are similar to ours, rather considered individual materials and thus used known values for hardness as constants, or estimated hardness values from known values of activation energy as an order-of-magnitude test of model viability.

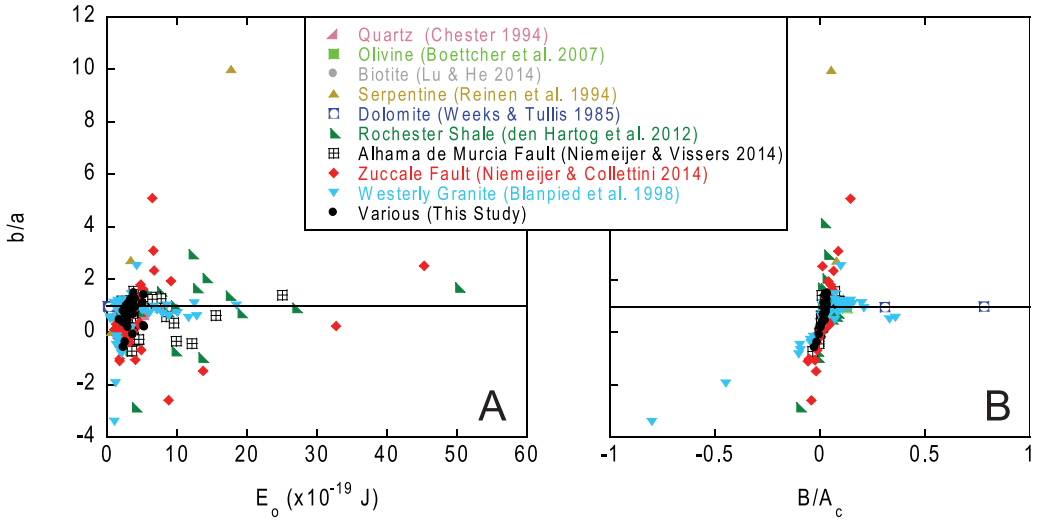

Figure 4. The ratio of the friction rate parameter b/a as a function of (a) the activation energy E_o, and (b) the normalized rate of growth of real contact area B/A_c. Data from this study (black circles) are compared with values calculated from other published friction studies noted in the legend.

In this current study, we use our wide-ranging suite of gouge materials to specifically investigate relationships between measureable friction parameters and the hardness H and activation volume Ω, where we consider H and Ω as separate parameters and evaluate them individually. We use previously published indentation hardness values for selected materials, which range from $H = 42$ MPa to 13 GPa. These values were obtained from data on talc [*Taylor*, 1949], the illite-smectite mixed-layer clay rectorite [*Zhang et al.*, 2009], kaolinite "macrocrystals" [*Mikowski et al.*, 2007], shale [*Bobko and Ulm*, 2008], mica schist [*Beste and Jacobson*, 2003; *Zhang et al.*, 2009], granite [*Beste and Jacobson*, 2003], orthoclase [*Taylor*, 1949], quartz [*Taylor*, 1949; *Westbrook*, 1958; *Oliver and Pharr*, 1992; *Beste and Jacobson*, 2003], and calcite [*Taylor*, 1949; *Beste and Jacobson*, 2003] (see Table 2). We use an average value if a range is given and assign these hardness values to the most compositionally similar gouges in our study (talc, montmorillonite, kaolinite, Rochester shale, biotite, Westerly granite, andesine, quartz, and the Scheggia gouge as calcite). We then calculate the activation volume Ω using these hardness values and our measured values of a for the selected samples according to equation (17).

We observe a general decrease in Ω with increasing a, as predicted from equation (17) (Figure 5); however note that this means that a is positively correlated with H, in contrast to the theory. This can be explained by the observation that H and Ω are strongly anti-correlated. Given the strong anti-correlation between H with Ω, the effect of Ω may overwhelm the relationship between a and H predicted by equation (17). We also observe that, with some scatter, lower values of b/a tend to occur in materials with large activation volumes and low hardness (Figure 5). Two materials tend to be outliers from the observed general trends: kaolinite, due to a very low hardness (reported by *Mikowski et al.* [2007]) and gouge from the Scheggia Thrust, which is composed mostly of calcite. Considering that data from dolomite are also outliers (Figure 4), it may be that calcite-rich materials have unusual properties causing a deviation from the theoretical framework. In general, the plastic activation

Table 2. Asperity Deformation Parameters

Sample	b/a	E_o (J)	B/A_c	H (GPa)[a]	Ω (nm^3)
Talc	−0.10	3.65E-19	−0.003	0.47	3.21
	0.15	3.04E-19	0.005		2.67
Montmorillonite	−0.40	2.63E-19	−0.015	0.73	1.68
	−0.60	2.36E-19	−0.024		1.51
Kaolinite	0.40	3.02E-19	0.013	0.042	21.76
	0.31	2.55E-19	0.012		18.39
Rochester Shale	0.17	5.35E-19	0.003	0.62	1.94
	0.22	5.24E-19	0.004		1.91
Biotite	0.35	2.28E-19	0.015	5.1–7.4	0.12
	0.46	1.78E-19	0.024		0.09
Westerly Granite	1.07	3.16E-19	0.032	8–9	0.06
	0.99	2.73E-19	0.034		0.06
Andesine	1.07	3.81E-19	0.027	7.1	0.09
	0.91	3.46E-19	0.025		0.08
Quartz sand	1.13	3.44E-19	0.031	10–13	0.05
	1.23	3.39E-19	0.035		0.05
Scheggia Thrust	1.47	3.81E-19	0.037	1–2	0.36
	1.21	3.83E-19	0.030		0.36

[a]Average values used where a range is given. See text for references.

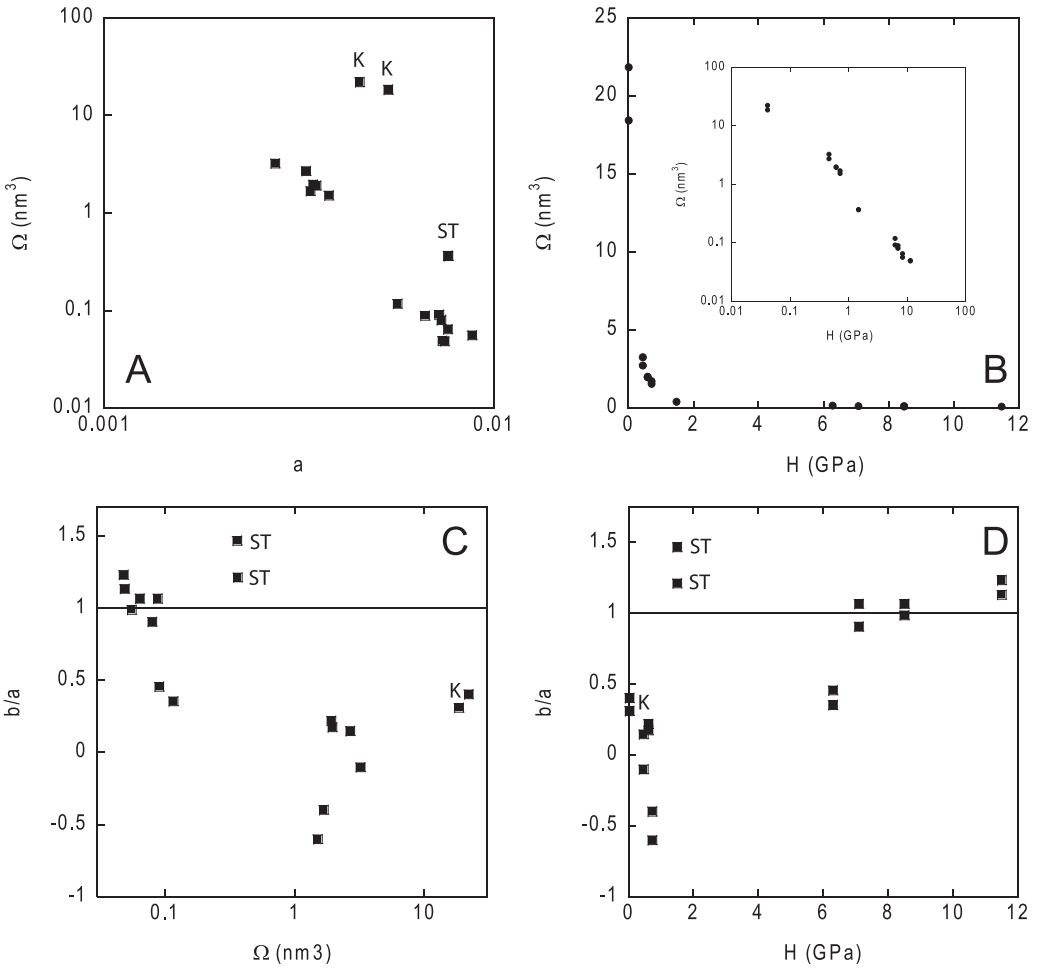

Figure 5. Activation volume Ω as a function of (a) the rate-dependent friction parameter a, and (B) hardness H for similar materials from previous data [*Taylor*, 1949; *Westbrook*, 1958; *Oliver and Pharr*, 1992; *Beste and Jacobson*, 2003; *Mikowski et al*., 2007; *Bobko and Ulm*, 2008; *Zhang et al*., 2009]. (b) Inset shows the same data on logarithmic scales. Velocity-dependence of friction presented as the ratio b/a is shown as a function of (c) the activation volume Ω, and (d) hardness H. Outliers to these trends are data for kaolinite (K) and fault gouge from the calcite-rich Scheggia Thrust (ST), as noted.

volume apparently plays a major role in controlling rate- and state-dependent friction; however the exceedingly small values (~0.05–20 nm^3) present some difficulty in associating it with macroscopic characteristics of fault gouge. We speculate that Ω scales with the number of individual bonds being rearranged, perhaps by dislocation glide, at a given time during plastic deformation of asperity contacts [e.g., *Griggs*, 1967; *Blacic and Christie*, 1984; *Mares and Kronenberg*, 1993; *Chen et al*., 2006; *Beeler et al*., 2007b].

Finally, although our data were obtained at constant temperature, we observe from equations (22) and (23) that b/a should depend inversely on temperature. However, we note that aside from the Boltzmann constant, all other variables should also be dependent on T and therefore the true dependence on T is the result of complicated interdependencies. We cannot rule out the possibility that the observed scaling between RSF parameters a, b, and μ_o is an artifact of other interdependence, for example between H, Ω and E_o. However, we feel that the broad range of material types studied and the consistency between the observed correlations and the theory based on thermally activated processes provides strong support for our proposed explanations.

5.2. How Grain Properties Control Friction

Several experimental studies have shown that the frictional behavior of fault zone materials is strongly controlled by mineral assemblage; specifically, gouges rich in phyllosilicate minerals tend to be weaker and frictionally stable [e.g., *Shimamoto and Logan*, 1981; *Brown et al*., 2003; *Ikari et al*., 2009, 2011a, 2011b,

Carpenter et al., 2012, 2016]. Because we observe that the healing rate β correlates with μ_o, we expect that weaker gouges should exhibit lower rates of healing, and in fact this is observed (Figure 6). Therefore, the strong positive correlation between b/a and B/A_c (Figure 4) can be explained by the idea that stronger minerals (higher μ_o, e.g., quartz or feldspar) exhibit higher healing rates than weaker minerals such as phyllosilicates. This is consistent with the expectation that particles of stronger material can have greater angularity, resulting in low A_c (originating from low $A_{c,o}$) which facilitates higher driving force for contact strengthening via contact area growth. In the case of phyllosilicate minerals, their platy habit means that the initial real area of contact is large, so the local normal stress σ_c will be correspondingly lower. In cases of very large A_c, σ_c may be significantly lower than H and thus the driving force for contact area growth would be low.

It may seem counterintuitive that the real area of contact is low for high-friction gouges, but high for gouges with low sliding friction. In the adhesion theory of friction, the frictional strength is directly proportional to the real area of contact [*Bowden and Tabor*, 1939, 1942, 1966], explaining generally how friction increases with time. However, while this relation may well describe changes in friction with contact area for an individual material, we propose that an assumption of proportionality between friction and real area of contact cannot be uniformly applied over a range of different materials having different grain surface properties.

One reason that frictional strength may not correlated with real area of contact over a range of materials is because in addition to net contact area, the quality of contact junctions is a crucial factor determining friction [*Bowden and Tabor*, 1939, 1942, 1966]. In these cases, chemical effects at contact junctions may be important [e.g., *Bureau et al*., 2002; *Renard et al*., 2012]. We focus here on a key difference between clays and other minerals such as quartz, feldspar, or calcite, which is that clay minerals have a net negative surface charge resulting from ionic substitutions in their atomic structure [*Sposito et al*., 1999; *Marry et al*., 2008]. Much of this charge is balanced by hydrogen bonding of water molecules to the mineral surface [*Marry et al*., 2008]. Such attractive forces between grains may trap water within contact junctions, producing heterogeneous contacts having areas of true atomic contact separated by regions of trapped water with lower strength. For the data of *Carpenter et al*. [2016], which were collected at relative humidity of 100%, a significant amount of water is bound to the surfaces of clays (Table 1). Several studies [*Morrow et al*., 2000; *Moore and Lockner*, 2004; *Ikari et al*., 2007; *Behnsen and Faulkner*, 2012] have shown that the presence of water significantly reduces the frictional strength of phyllosilicate gouges. For clay-poor materials this weakening effect is smaller, for example in friction studies using quartz sand [*Frye and Marone*, 2002], bare granite surfaces [*Dieterich and Conrad*, 1984], and soda-lime glass beads [*Scuderi et al*., 2014] but also some higher-grade phyllosilicate minerals such as mica and talc [*Morrow et al*., 2000] which are hydrophobic [*Giese et al*., 1996]. However, the importance of water for these materials is highlighted in experiments under truly dry conditions, which show that the absence of water eliminates healing in quartz, bare granite and glass beads. This supports the inference that water-assisted creep is the likely mechanism of fault healing [e.g., *Dieterich and Conrad*, 1984; *Frye and Marone*, 2002; *Scuderi et al*., 2014].

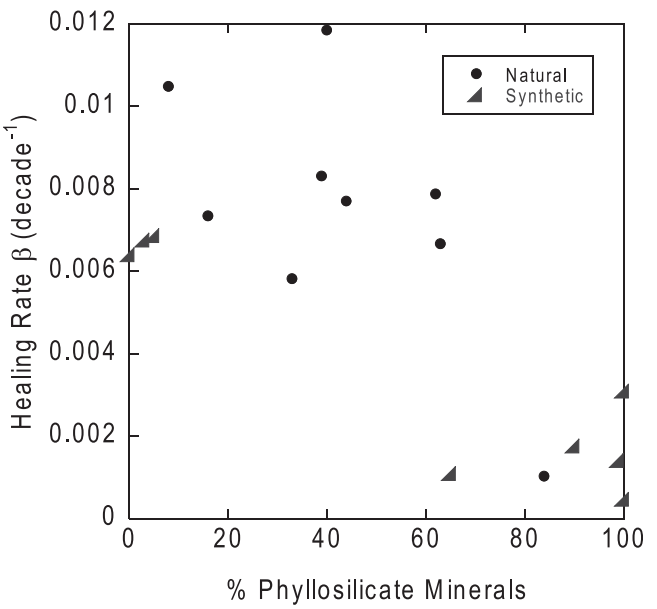

Figure 6. Summary of data from *Carpenter et al*. [2016] showing healing rate β as a function of phyllosilicate mineral content for natural and synthetic fault gouges. Note that healing rate decreases with increasing phyllosilicate content.

We compare RSF parameters from two subsaturated clay-rich samples with samples sheared under fluid-saturated conditions at controlled pore pressure. Figure 7 compares a synthetic gouge, Rochester shale [*Ikari et al*., 2009], with

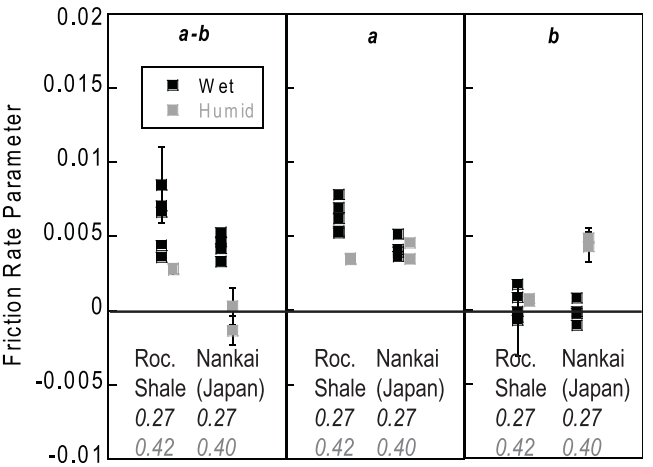

Figure 7. Comparison of $a-b$, a, and b for "wet" (water saturated) and "humid" (subsaturated) conditions and two fault gouges: Rochester shale and the Nankai Trough décollement zone. The values of base friction μ_o are given for each material under wet and humid conditions.

a natural gouge from the plate boundary décollement in the Nankai Trough subduction zone [*Ikari and Saffer*, 2011]. Note that these two gouges exhibit nearly identical frictional strength. It is evident that the water saturation lowers the friction coefficient and also increases $a-b$. Elevated $a-b$ values in water-saturated samples can be attributed to lower values of b (e.g., for Nankai), as expected.

The data of Figure 7 also highlight an interesting feature of the friction direct effect: the parameter a is larger in wet samples (e.g., Rochester shale). The mechanics controlling a are not well understood [e.g., *Beeler et al*., 2007b; *King and Marone*, 2012; *Behnsen and Faulkner*, 2012], but equation (17) suggests that an increase in a is associated with a reduction in hardness and/or the activation volume. Lower hardness can be explained by hydrolytic weakening: a reduction in activation volume may be due to bond rearrangement being restricted to mineral-mineral portions of the asperity contact and inhibited where water molecules are trapped. In terms of friction, H and/or Ω also control the minimum activation energy E_o (equation (16)), therefore an increase in a would be driven by a large reduction in E_o compared to μ_o (equation (20)). This is consistent with the idea of lubrication by trapped water molecules, requiring less force for displacement at asperity contacts [e.g., *Israelachvili et al*., 1988; *Morrow et al*., 2000].

6. Implications for Slip Instability in the Upper Crust

Our analysis suggests that an increasing tendency for seismogenesis with depth, from Earth's surface to the base of the seismogenic zone, should be associated with an increase in the rate of shear strength increase (the frictional aging rate) at grain-scale asperities. Two factors appear to be particularly important for dictating the contact area growth rate: (1) the absolute value of the contact area, which is highly dependent on grain properties (e.g., phyllosilicates vs. framework minerals), and (2) a competition between the material hardness and the activation volume of plastic deformation. Although our experiments were conducted under brittle faulting conditions, we explore how a model employing asperity contact mechanics also may apply to faults at higher pressure and temperature conditions.

To first order, an increase in normal force with increasing depth would result in larger local normal stresses driving contact area growth [e.g., *Logan and Teufel*, 1986]. This supports a correlation between normal force and seismic coupling in subduction zones inferred from geodetic measurements [*Scholz and Campos*, 1995, 2012]. Increasing temperature with depth should also drive higher time-dependent strengthening rates if asperity contact shear strength follows an Arrhenius relationship as assumed here, by favoring large activation volumes. However, parameter interdependence makes the true depth-dependent effect of temperature complicated. For example, H is expected to decrease with T as observed for quartz [*Westbrook*, 1958; *Evans*, 1984], but B and Ω may increase with T, and μ_o may increase or decrease depending on the temperature range and material composition [*Stesky*, 1978; *Blanpied et al*., 1991, 1998; *Moore and Lockner*, 2008; *Van Diggelen et al*., 2009; *den Hartog et al*., 2012; *King and Marone*, 2012; *Saffer et al*., 2012].

Increasing pressure and temperature drives specific mechanisms that result in time-dependent strengthening. One important mechanism is pressure solution, or mineral dissolution followed by rapid local precipitation is a mechanism that would result in rapid increases in both contact area but also cohesion [*Rutter*, 1983; *Schutjens*, 1991; *Scholz et al*., 1995; *Bos and Spiers*, 2001, 2002; *Niemeijer and Spiers*, 2002; *Beeler and Hickman*, 2004; *Niemeijer et al*., 2008]. Cohesive strengthening by grain welding or suturing becomes important at seismogenic conditions by increasing contact quality, primarily for quartz or calcite which function

as cements [*Towe*, 1962; *Sample*, 1990; *Bernabé et al*., 1992]; which has been demonstrated experimentally [*Tenthorey and Cox*, 2006]. For phyllosilicates, a mechanism for strengthening would be an inhibition of the tendency for water molecules to bond to mineral surfaces. Temperature-dependent clay dehydration [*Bird*, 1984; *Pytte and Reynolds*, 1989; *Ikari et al*., 2007], transformation of hydrophilic clay minerals to hydrophobic micas [*Árkai*, 2002; *van de Kamp*, 2008] and/or an increase in charge-neutral quartz content, via silica release from clay transformation reactions [*Towe*, 1962; *van de Kamp*, 2008], may drive this effect.

At higher temperatures and pressures consistent with the downdip limit of seismogenesis, creep deformation may become so rapid that the real area of frictional contact reaches a limit controlled by the integrity of the mineral crystal structure, and would saturate. This would cause the contact area growth rate to drop to zero. In this case, the RSF parameter b would become zero or negative, which would yield velocity-strengthening frictional behavior. This scenario is consistent with laboratory results for temperatures high enough to induce crystal plasticity in quartz [*Chester and Higgs*, 1992; *Karner et al*., 1997; *Blanpied et al*., 1998]. *Chester and Higgs* [1992] also noted that the experiments in which $b \leq 0$ exhibited nearly complete porosity loss, indicating complete saturation of contact area. If the entire fault zone is deforming plastically, the activation volume may also saturate while the hardness and friction decline, favoring stable creep. Phyllosilicate minerals at elevated pressures and temperatures are expected to occur as strongly foliated mica or chlorite schists. Previous experiments in which this foliation has been preserved have shown that mica schists are also consistently velocity-strengthening with low to negative values of b [*Ikari et al*., 2011b], thus their time-dependent strengthening rates will likely be correspondingly low at depths greater than the seismogenic zone.

7. Conclusions

We use laboratory data to demonstrate relationships between the rate- and state- friction parameters a and b, the reference coefficient of sliding friction μ_o, and the rate of frictional strengthening β. We demonstrate that for a wide range of natural and analogue fault gouges, the combined results of slide-hold-slide and velocity-step tests suggest that high rates of frictional healing, which cause high rates of interseismic fault strengthening, also result in high values of the friction evolution parameter b, and therefore low, negative, values of $a-b$. We present a microphysical model, which demonstrates that under low pressure and temperature conditions, these parameters also correlate with the absolute values of friction, such that strong fault gouges are likely to be supported by relatively smaller real areas of contact compared to materials with lower friction and thus experience high rates of contact area growth. The rate of frictional strengthening depends on material hardness and the activation volume of plastic deformation. Furthermore, we suggest that materials with low friction readily collapse into a state of high overall contact area that does not easily increase with time. Contact stresses may also be lowered by the presence of water bound to mineral surfaces. With increasing depth in the upper crust, seismicity is enhanced by increasing normal force and contact area growth rate facilitated by a combination of decreasing hardness and increasing activation volume with temperature. Our results suggest that at the downdip limit of the seismogenic zone, velocity-strengthening frictional behavior is expected because contact area approaches saturation so that the rate of contact area growth becomes negligible. Collectively, our results demonstrate that RSF laws can explain frictional strength evolution at all scales, including time and velocity dependence, and that the micromechanics controlling frictional strength can explain macroscopic fault slip behavior in the crust.

Acknowledgments
We thank Eran Bouchbinder, Yohai Bar-Sinai, Michael Aldam and André Niemeijer for helpful discussions, Nick Beeler and Anne Pluymakers for commenting on an early version of this manuscript, and two anonymous reviewers for helpful suggestions. This work was supported by NSF grants EAR-054570, EAR-0746192, and OCE-0648331 to CM. All data used in this article are available by contacting the corresponding author.

References

Árkai, P. (2002), Phyllosilicates in very low-grade metamorphism: Transformation to micas, *Rev. Mineral. Geochem.*, *46*, 463–478, doi: 10.2138/rmg.2002.46.11.

Atkinson, B. K. (1984), Subcritical crack growth in geological materials, *J. Geophys. Res.*, *89*, 4077–4114.

Bar-Sinai, Y., R. Spatschek, E. A. Brener, and E. Bouchbinder (2014), On the velocity-strengthening behavior of dry friction, *J. Geophys. Res. Solid Earth*, *119*, 1738–1748, doi:10.1029/2013JB010586.

Baumberger, T. (1997), Contact dynamics and friction at a solid-solid interface: Material versus statistical aspects, *Solid State Commun.*, *102*, 175–185.

Baumberger, T., and C. Caroli (2006), Solid friction from stick-slip down to pinning and aging, *Adv. Phys.*, *55*, 279–348.

Baumberger, T., P. Berthoud, and C. Caroli (1999), Physical analysis of the state- and rate-dependent friction law. II. Dynamic friction, *Phys. Rev. B*, *60*, 3928–3939.

Bayart, E., A. M. Rubin, and C. Marone (2006), Evolution of fault friction following large velocity jumps, *Eos Trans. AGU*, *87*(52), Fall Meet. Suppl., Abstract S31A-0180.

Beeler, N. M. (2007), Laboratory-observed faulting in intrinsically and apparently weak materials, in *The Seismogenic Zone of Subduction Thrust Faults*, edited by T. H. Dixon and J. C. Moore, pp. 370–449, Columbia Univ. Press, N. Y.
Beeler, N. M., and S. H. Hickman (2004), Stress-induced, time-dependent fracture closure at hydrothermal conditions, *J. Geophys. Res.*, *109*, B02211, doi:10.1029/2002JB001782.
Beeler, N. M., T. E. Tullis, and J. D. Weeks (1994), The roles of time and displacement in the evolution effect in rock friction, *Geophys. Res. Lett.*, *21*, 1987–1990.
Beeler, N. M., T. E. Tullis, M. L. Blanpied, and J. D. Weeks (1996), Frictional behavior of large displacement experimental faults, *J. Geophys. Res.*, *101*, 8697–8715.
Beeler, N. M., T. E. Tullis, A. K. Kronenberg, and L. A. Reinen (2007), The instantaneous rate dependence in low temperature laboratory rock friction and rock deformation experiments, *J. Geophys. Res.*, *112*, B07310, doi:10.1029/2005JB003772.
Behnsen, J., and D. R. Faulkner (2012), The effect of mineralogy and effective normal stress on frictional strength of sheet silicates, *J. Struct. Geol.*, *42*, 49–61.
Bernabé, Y., D. T. Fryer and J. A. Hayes (1992), The effect of cement on the strength of granular rocks, *Geophys. Res. Lett.*, *19*, 1511–1514.
Beste, U., and S. Jacobson (2003), Micro scale hardness distribution of rock types related to rock drill wear, *Wear*, *254*, 1147–1154.
Bhattacharya, P., A. M. Rubin, E. Bayart, H. M. Savage, and C. Marone (2015), Critical evaluation of state evolution laws in rate and state friction: Fitting large velocity steps in simulated fault gouge with time-, slip- and stress-dependent constitutive laws, *J. Geophys. Res. Solid Earth*, *120*, 6365–6385, doi:10.1002/2015JB012437.
Bird, P. (1984), Hydration-phase diagrams and friction of montmorillonite under laboratory and geologic conditions with implications for shale compaction, slope stability, and strength of fault gouge, *Tectonophysics*, *107*, 235–260.
Bizzarri, A. (2011), On the deterministic description of earthquakes, *Rev. Geophys.*, *49*, RG3002, doi:10.1029/2011RG000356.
Blacic, J. D., and J. M. Christie (1984), Plasticity and hydrolytic weakening of quartz single crystals, *Geophys. Res. Lett.*, *89*, 4223–4239.
Blanpied, M. L., D. A. Lockner, and J. D. Byerlee (1991), Fault stability inferred from granite sliding experiments at hydrothermal conditions, *Geophys. Res. Lett.*, *18*, 609–612.
Blanpied, M. L., C. J. Marone, D. A. Lockner, J. D. Byerlee, and D. P. King (1998), Quantitative measure of the variation in fault rheology due to fluid-rock interactions, *J. Geophys. Res.*, *103*, 9691–9712.
Bobko, C., and F.-J. Ulm (2008), The nano-mechanical morphology of shale, *Mech. Mater.*, *40*, 318–337, doi:10.1016/j.mechmat.2007.09.006.
Boettcher, M. S., G. Hirth, and B. Evans (2007), Olivine friction at the base of oceanic seismogenic zones, *J. Geophys. Res.*, *112*, B01205, doi: 10.1029/2006JB004301.
Bos, B., and C. J. Spiers (2001), Experimental investigation into the microstructural and mechanical evolution of phyllosilicate-bearing rock under conditions favoring pressure solution, *J. Struct. Geol.*, *23*, 1187–1202.
Bos, B., and C. J. Spiers (2002), Fluid-assisted healing processes in gouge-bearing faults: Insights from experiments on a rock analogue system, *Pure Appl. Geophys.*, *159*, 2537–2566.
Bowden, F. P., and D. Tabor (1939), The area of contact between stationary and between moving surfaces, *Proc. R. Soc. London, Ser. A*, *169*, 391–413.
Bowden, F. P., and D. Tabor (1942), Mechanism of metallic friction, *Nature*, *150*, 197–199.
Bowden, F. P., and D. Tabor (1966), Friction, lubrication and wear: A survey of work during the last decade, *Br. J. Appl. Phys.*, *17*, 1521–1544.
Brace, W. F. (1972), Laboratory studies of stick-slip and their application to earthquakes, *Tectonophysics*, *14*, 189–200.
Brechet, Y., and Y. Estrin (1994), The effect of strain rate sensitivity on dynamic friction of metals, *Scripta Metal. Materialia*, *30*, 1449–1454.
Brockley, C. A., and H. R. Davis (1968), The time-dependence of static friction, *J. Lubric. Technol.*, *90*, 35–41.
Brown, K. M., A. Kopf, M. B. Underwood, and J. L. Weinberger (2003), Compositional and fluid pressure controls on the state of stress on the Nankai subduction thrust: A weak plate boundary, *Earth Planet. Sci. Lett.*, *214*, 589–603.
Bureau, L., T. Baumberger, and C. Caroli (2002), Rheological aging and rejuvenation in solid frictional contacts, *Eur. Phys. J. E*, *8*, 331–337.
Byerlee, J. D. (1970), The mechanics of stick-slip, *Tectonophysics*, *9*, 475–486.
Cao, T., and K. Aki (1986), Seismicity simulation with a rate- and state-dependent friction law, *Pure Appl. Geophys.*, *124*, 487–513.
Carpenter, B. M., D. M. Saffer, and C. Marone (2012), Frictional properties and sliding stability of the San Andreas fault from deep drill core, *Geology*, *40*, 759–762, doi:10.1130/G33007.1.
Carpenter, B. M., M. J. Ikari, and C. Marone (2016), Laboratory observations of time-dependent frictional strengthening and stress relaxation in natural and synthetic fault gouges, *J. Geophys. Res. Solid Earth*, *121*, 1183–1201, doi:10.1002/2015JB012136.
Chen, J., L. Lu, and K. Lu (2006), Hardness and strain rate sensitivity of nanocrystalline Cu, *Scripta Materialia*, *54*, 1913–1918.
Chester, F. M. (1994), Effects of temperature on friction: Constitutive equations and experiments with quartz gouge, *J. Geophys. Res.*, *99*, 7247–7261.
Chester, F.,M., and N. G. Higgs (1992), Multimechanism friction constitutive model for ultrafine quartz gouge at hypocentral locations, *J. Geophys. Res.*, *97*, 1859–1870.
den Hartog, S. A. M., and C. J. Spiers (2013), Influence of subduction zone conditions and gouge composition on frictional slip stability of megathrust faults, *Tectonophysics*, *600*, 75–90.
den Hartog, S. A. M., and C. J. Spiers (2014), A microphysical model for fault gouge friction applied to subduction megathrusts, *J. Geophys. Res. Solid Earth*, *119*, 1510–1529, doi:10.1002/2013JB010580.
den Hartog, S. A. M., A. R. Niemeijer, and C. J. Spiers (2012), New constraints on megathrust slip stability under subduction zone P-T conditions, *Earth Planet. Sci. Lett.*, *353-354*, 240–252, doi:10.1016/j.epsl.2012.08.022.
Dieterich, J. H. (1972), Time-dependent friction in rocks, *J. Geophys. Res.*, *77*, 3690–3697.
Dieterich, J. H. (1978), Time-dependent friction and the mechanics of stick-slip, *Pure Appl. Geophys.*, *116*, 790–806.
Dieterich, J. H. (1979), Modeling of rock friction 1. Experimental results and constitutive equations, *J. Geophys. Res.*, *84*, 2161–2168.
Dieterich, J. H. (1981), Constitutive properties of faults with simulated gouge, in *Mechanical Behavior of Crustal Rocks, Geophys. Monogr. Ser., 24*, edited by N. L. Carter et al., pp. 102–120, AGU, Washington, D. C.
Dieterich, J. H. (1992), Earthquake nucleation on faults with rate- and state-dependent strength, *Tectonophysics*, *211*, 115–134.
Dieterich, J. H., and G. Conrad (1984), Effect of humidity on time- and velocity-dependent friction in rocks, *J. Geophys. Res.*, *89*, 4196–4202.
Dieterich, J. H., and B. D. Kilgore (1994), Direct observation of frictional contacts: New insights for state-dependent properties, *Pure Appl. Geophys.*, *143*, 283–302.
Dieterich, J. H., and B. D. Kilgore (1996), Imaging surface contacts: Power law contact distributions and contact stresses in quartz, calcite, glass and acrylic plastic, *Tectonophysics*, *256*, 219–239.
Engelder, J. T., and C. H. Scholz (1976), The role of asperity indentation and ploughing in rock friction–-II. Influence of relative hardness and normal load, *Int. J. Rock Mech. Min. Sci. Geomech. Abstr.*, *13*, 155–163.

Estrin, Y., and Y. Bréchet (1996), On a model of frictional sliding, *Pure Appl. Geophys.*, *147*, 745–762.
Evans, B. (1984), The effect of temperature and impurity content in indentation hardness of quartz, *J. Geophys. Res.*, *89*, 4213–4222.
Friedman, M., and N. G. Higgs (1981), Calcite fabrics in experimental shear zones, in *Mechanical Behavior of Crustal Rocks, Geophys. Monogr. Ser., 24*, edited by N. L. Carter et al., pp. 11–27, AGU, Washington, D. C.
Frye, K. M., and C. Marone (2002), Effect of humidity on granular friction at room temperature, *J. Geophys. Res.*, *107*(B11), 2309, doi:10.1029/2001JB000654.
Giese, R. F., W. Wu, and C. J. van Oss (1996), Surface and electrokinetic properties of clays and other mineral particles, untreated and treated with organic or inorganic compounds, *J. Dispersion Sci. Tech.*, *17*, 527–547.
Goldsby, D. L., A. Rar, G. M. Pharr, and T. E. Tullis (2004), Nanoindentation creep of quartz, with implications for rate- and state-variable friction laws relevant to earthquake mechanics, *J. Mater. Res.*, *19*, 357–365.
Griggs, D. (1967), Hydrolytic weakening of quartz and other silicates, *Geophys. J. R. Astron. Soc.*, *14*, 19–31.
Gu, J.-C., J. R. Rice, A. L. Ruina, and S. T. Tse (1984), Slip motion and stability of a single degree of freedom elastic system with rate and state dependent friction, *J. Mech. Phys. Solids*, *32*, 167–196.
Handin, J. (1969), On the Coulomb-Mohr failure criterion, *J. Geophys. Res.*, *74*, 5343–5348.
Heslot, F., T. Baumberger, B. Perrin, B. Caroli, and C. Caroli (1994), Creep, stick-slip, and dry-friction dynamics: Experiments and a heuristic model, *Phys. Rev. E*, *49*, 4973–4987.
Hirth, G., C. Teyssier and W. J. Dunlap (2001), An evaluation of quartzite flow laws based on comparisons between experimentally and naturally deformed rocks, *Int. J. Earth Sci.*, *90*, 77–87.
Ibanez, W. D., and A. K. Kronenberg (1993), Experimental deformation of shale: Mechanical properties and microstructural indicators of mechanisms, *Int. J. Rock Mech. Min. Sci. Geomech. Abstr.*, *30*, 723–734.
Ikari, M. J., and A. J. Kopf (2011), Cohesive strength of clay-rich sediment, *Geophys. Res. Lett.*, *38*, L16309, doi:10.1029/2011GL047918.
Ikari, M. J., and D. M. Saffer (2011), Comparison of frictional strength and velocity dependence between fault zones in the Nankai accretionary complex, *Geochem. Geophys. Geosyst.*, *12*, Q0AD11, doi:10.1029/2010GC003442.
Ikari, M. J., D. M. Saffer, and C. Marone (2007), Effect of hydration state on the frictional properties of montmorillonite-based fault gouge, *J. Geophys. Res.*, *112*, B06423, doi:10.1029/2006JB004748.
Ikari, M. J., D. M. Saffer, and C. Marone (2009), Frictional and hydrologic properties of clay-rich fault gouge, *J. Geophys. Res.*, *114*, B05409, doi:10.1029/2008JB006089.
Ikari, M. J., C. Marone, and D. M. Saffer (2011a), On the relation between fault strength and frictional stability, *Geology*, *39*, 83–86, doi:10.1130/G31416.1.
Ikari, M. J., A. R. Niemeijer and C. Marone (2011b), The role of fault zone fabric and lithification state on frictional strength, constitutive behavior, and deformation microstructure, *J. Geophys. Res.*, *116*, B08404, doi:10.1029/2011JB008264.
Ikari, M. J., M. W. Knuth, C. Marone and D. M. Saffer (2012), Data report: Frictional healing and compressibility of sheared sediment from fault zones, Sites C0004 and C0007, in *Proceedings of Integrated Ocean Drilling Program, 314/315/316*, edited by M. Kinoshita et al., Integrated Ocean Drill. Program Manage. Int. Inc., Washington, D. C., doi:10.2204/iodp.proc.314315316.219.2012.
Israelachvili, J. N., P. M. McGuiggan, and A. M. Homola (1988), Dynamic properties of molecularly thin liquid films, *Science*, *240*, 189–191.
Karner, S. L., and C. Marone (2001), Frictional restrengthening in simuated fault gouge: Effect of shear load perturbations, *J. Geophys. Res. 106*, 19,319–19,337.
Karner, S. L., C. Marone, and B. Evans (1997), Laboratory study of fault healing and lithification in simulated fault gouge under hydrothermal conditions, *Tectonophysics*, *277*, 41–55.
King, D. S. H., and C. Marone (2012), Frictional properties of olivine at high temperature with applications to the strength and dynamics of the oceanic lithosphere, *J. Geophys. Res.*, *117*, B12203, doi:10.1029/2012JB009511.
Kronenberg, A. K., S. H. Kirby, and J. Pinkston (1990), Basal slip and mechanical anisotropy of biotite, *J. Geophys. Res.*, *95*, 19,257–19,278.
Leeman, J. R., M. M. Scuderi, C. Marone, and D. M. Saffer (2015), On the origin and evolution of electrical signals during frictional stick slip in sheared granular matter, *Granular Matter*, *17*, 447–457, doi:10.1007/s10035-015-0565-1.
Li, Q., T. E. Tullis, D. Goldsby, and R. W. Carpick (2011), Frictional ageing from interfacial bonding and the origins of rate and state friction, *Nature*, *480*, 233–236, doi:10.1038/nature10589.
Liu, Y., and J. R. Rice (2005), Aseismic slip transients emerge spontaneously in three-dimensional rate and state modeling of subduction earthquake sequences, *J. Geophys. Res.*, *110*, B08397, doi:10.1029/2004JB003424.
Lockner, D. (1993), Room temperature creep in saturated granite, *J. Geophys. Res.*, *98*, 475–487.
Logan, J. M., and L. W. Teufel (1986), The effect of normal stress on the real area of contact during frictional sliding in rocks, *Pure Appl. Geophys.*, *124*, 471–485.
Lu, Z., and C. He (2014), Frictional behavior of simulated biotite fault gouge under hydrothermal conditions, *Tectonophysics*, *622*, 62–80, doi:10.1016/j.tecto.2014.03.002.
Mair, K., and C. Marone (1999), Friction of simulated fault gouge for a wide range of velocities and normal stresses, *J. Geophys. Res.*, *104*, 28,899–28,914.
Mares, V. M., and A. K. Kronenberg (1993), Experimental deformation of muscovite, *J. Struct. Geol.*, *15*, 1061–1075.
Marone, C. (1998a), Laboratory-derived friction laws and their application to seismic faulting, *Annu. Rev. Earth Planet. Sci.*, *26*, 643–696.
Marone, C. (1998b), The effect of loading rate on static friction and the rate of fault healing during the earthquake cycle, *Nature*, *391*, 69–72.
Marone, C., and D. M. Saffer (2015), The mechanics of frictional healing and slip instability during the seismic cycle, in *Treatise on Geophysics*, 2nd ed., edited by G. Schubert, pp. 111–138, doi:10.1016/B978-0-444-53802-4.00092-0.
Marone, C., C. B. Raleigh, and C. H. Scholz (1990), Frictional behavior and constitutive modeling of simulated fault gouge, *J. Geophys. Res.*, *95*, 7007–7025.
Marone, C. J., C. H. Scholz, and R. Bilham (1991), On the mechanics of earthquake afterslip, *J. Geophys. Res.*, *96*, 8441–8452.
Marry, V., B. Rotenberg, and P. Turq (2008), Structure and dynamics of water at a clay surface from molecular dynamics simulation, *Phys. Chem. Chem. Phys.*, *10*, 4802–4813.
Masuda, T., T. Hiraga, H. Ikei, H. Kanda, Y. Kugimiya and M. Akizuki (2000), Plastic deformation of quartz at room temperature: A Vickers nano-indenation test, *Geophys. Res. Lett.*, *27*, 2773–2776.
Mikowski, A., P. Soares, F. Wypych, J. E. F. C. Gardolinski, and C. M. Lepienski (2007), Mechanical properties of kaolinite 'macro-crystals,' *Philos. Mag. A*, *87*, 4445–4459, doi:10.1080/14786430701550394.
Moore, D. E., and D. A. Lockner (2004), Crystallographic controls on the frictional behavior of dry and water-saturated sheet structure minerals, *J. Geophys. Res.*, *109*, B03401, doi:10.1029/2003JB002582.

Moore, D. E., and D. A. Lockner (2008), Talc friction in the temperature range 25°-400°C: Relevance for fault-zone weakening, *Tectonophysics*, *449*, 120–132.
Morrow, C. A., D. E. Moore, and D. A. Lockner (2000), The effect of mineral bond strength and adsorbed water on fault gouge frictional strength, *Geophys. Res. Lett.*, *27*, 815–818.
Nakatani, M., and C. H. Scholz (2004a), Frictional healing of quartz gouge under hydrothermal conditions: 1. Experimental evidence for solution transfer healing mechanism, *J. Geophys. Res.*, *109*, B07201, doi:10.1029/2001JB001522.
Nakatani, M., and C. H. Scholz (2004b), Frictional healing of quartz gouge under hydrothermal conditions: 2. Quantitative interpretation with a physical model, *J. Geophys. Res.*, *109*, B07202, doi:10.1029/2003JB002938.
Niemeijer, A. R., and C. Collettini (2014), Frictional properties of a low-angle normal fault under in situ conditions: Thermally-activated velocity weakening, *Pure Appl. Geophys.*, *171*, 2641–2664, doi:10.1007/s00024-013-0759-6.
Niemeijer, A. R., and C. J. Spiers (2002), Compaction creep of quartz-muscovite mixtures at 500°C: Preliminary results on the influence of muscovite on pressure solution, in *Deformation Mechanisms, Rheology and Tectonics: Current Status and Future Perspectives*, edited by S. de Meer et al., *Geol. Soc. London Spec. Publ.*, *200*, 61–71, doi:10.1144/GSL.SP.2001.200.01.04.
Niemeijer, A. R., and C. J. Spiers (2006), Velocity dependence of strength and healing behavior in simulated phyllosilicate-bearing fault gouge, *Tectonophysics*, *427*, 231–253.
Niemeijer, A. R., and C. J. Spiers (2007), A microphysical model for strong velocity-weakening in phyllosilicate-bearing fault gouges, *J. Geophys. Res.*, *112*, B10405, doi:10.1029/2007JB005008.
Niemeijer, A. R., and R. L. M. Vissers (2014), Earthquake rupture propagation inferred from the spatial distribution of fault rock frictional properties, *Earth Planet. Sci. Lett.*, *396*, 154–164, doi:10.1016/j.epsl.2014.04.010.
Niemeijer, A. R., C. Marone, and D. Elsworth (2008), Healing of simulated fault gouges aided by pressure solution: Results from rock analogue experiments, *J. Geophys. Res.*, *113*, B04204, doi:10.1029/2007JB005376.
Okubo, P. G. (1989), Dynamic rupture modeling with laboratory-derived constitutive relations, *J. Geophys. Res.*, *94*, 12,321–12,335.
Oliver, W. C., and G. M. Pharr (1992), An improved technique for determining hardness and elastic modulus using load and displacement sensing indentation experiments, *J. Mater. Res.*, *7*, 1564–1583.
Perfettini, H., and J.-P. Avouac (2004), Postseismic relaxation driven by brittle creep: A possible mechanism to reconcile geodetic measurements and the decay rate of aftershocks, application to the Chi-Chi earthquake, Taiwan, *J. Geophys. Res.*, *109*, B02304, doi:10.1029/2003JB002488.
Perfettini, H., and J.-P. Avouac (2007), Modeling afterslip and aftershocks following the 1992 Landers earthquake, *J. Geophys. Res.*, *112*, B07409, doi:10.1029/JB2006JB004399.
Persson, B. J. N. (1999), Sliding friction, *Surf. Sci. Rep.*, *33*, 83–119.
Pytte, A. M., and R. C. Reynolds (1989), The thermal transition of smectite to illite, in *Thermal History of Sedimentary Basins: Methods and Case Studies*, edited by N. D. Naeser and T. H. McCulloch, pp. 33–40, Springer, N. Y.
Rabinowicz, E. (1951), The nature of the static and kinetic coefficients of friction, *J. Appl. Phys.*, *22*, 1373–1379.
Rabinowicz, E. (1956), Stick and slip, *Sci. Am.*, *194*, 109–119.
Rathbun, A. P., and C. Marone (2010), Effect of strain localization on frictional behavior of sheared granular materials, *J. Geophys. Res.*, *115*, B01204, doi:10.1029/2009/JB006466.
Reinen, L. A., and J. D. Weeks (1993), Determination of rock friction constitutive parameters using an iterative least-squares inversion method, *J. Geophys. Res.*, *98*, 15,937–15,950.
Reinen, L. A., J. D. Weeks, and T. E. Tullis (1994), The frictional behavior of lizardite and antigorite serpentinites: Experiments, constitutive models, and implications for natural faults, *Pure Appl. Geophys.*, *143*, 317–358.
Renard, F., S. Beaupretre, C. Voisin, D. Zigone, T. Candela, D. K. Dysthe, and J.-P. Gratier (2012), Strength evolution of a reactive frictional interface is controlled by the dynamics of contacts and chemical effects, *Earth Planet. Sci. Lett.*, *341–344*, 20–34.
Rice, J. R., and A. L. Ruina (1983), Stability of steady frictional slipping, *J. Appl. Mech.*, *50*, 343–349.
Rice, J. R., N. Lapusta, and K. Ranjith (2001), Rate and state dependent friction and the stability of sliding between elastically deformable solids, *J. Mech. Phys. Solids*, *49*, 1865–1898.
Richardson, E., and C. Marone (1999), Effects of normal stress vibrations on frictional healing, *J. Geophys. Res.*, *104*, 28,859–28,878.
Rubin, A. M. (2008), Episodic slow slip events and rate-and-state friction, *J. Geophys. Res.*, *113*, B11414, doi:10.1029/2008JB005642.
Rubin, A. M. (2011), Designer friction laws for bimodal slow slip propagation speeds, *Geochem. Geophys. Geosyst. 12*, Q04007, doi:10.1029/2010GC003386.
Rubin, A. M., and J.-P. Ampuero (2005), Earthquake nucleation on (aging) rate and state faults, *J. Geophys. Res.*, *110*, B11312, doi:10.1029/2005JB003686.
Ruina, A. (1983), Slip instability and state variable friction laws, *J. Geophys. Res.*, *88*, 10,359–10,370.
Rutter, E. H. (1983), Pressure solution in nature, theory and experiment, *J. Geol. Soc. London*, *140*, 725–740.
Saffer, D. M., and C. Marone (2003), Comparison of smectite- and illite-rich gouge frictional properties: Application to the updip limit of the seismogenic zone along subduction megathrusts, *Earth Planet. Sci. Lett.*, *215*, 219–235.
Saffer, D. M., D. A. Lockner, and A. W. McKiernan (2012), Effects of smectite to illite transformation on the frictional strength and sliding stability of intact marine mudstones, *Geophys. Res. Lett.*, *39*, L11304, doi:10.1029/2012GL051761.
Sample, J. C. (1990), The effect of carbonate cementation of underthrust sediments on deformation styles during underplating, *J. Geophys. Res.*, *95*, 9111–9121.
Scholz, C. H. (2002), *The Mechanics of Earthquakes and Faulting*, 2nd ed., Cambridge Press, N. Y.
Scholz, C. H., and J. Campos (1995), On the mechanism of seismic decoupling and back arc spreading at subduction zones, *J. Geophys. Res.*, *100*, 22,103–22,115.
Scholz, C. H., and J. Campos (2012), The seismic coupling of subduction zones revisited, *J. Geophys. Res.*, *117*, B05310, doi:10.1029/2011JB009003.
Scholz, C. H., and J. T. Engelder (1976), The role of asperity indentation and ploughing in rock friction – I. Asperity creep and stick-slip, *Int. J. Rock Mech. Min. Sci. Geomech. Abstr.*, *13*, 149–154.
Scholz, C. H., A. Léger and S. L. Karner (1995), Experimental diagenesis: Exploratory results, *Geophys. Res. Lett.*, *22*, 719–722.
Schutjens, P. M. T. M. (1991), Experimental compaction of quartz sand at low effective stress and temperature conditions, *J. Geol. Soc. London*, *148*, 527–539.
Scruggs, V. J., and T. E. Tullis (1998), Correlation between velocity dependence of friction and strain localization in large displacement experiments on feldspar, muscovite and biotite gouge, *Tectonophysics*, *295*, 15–40.
Scuderi, M. M., B. M. Carpenter, and C. Marone (2014), Physicochemical processes of frictional healing: Effects of water on stick-slip stress drop and friction of granular fault gouge, *J. Geophys. Res. Solid Earth*, *119*, 4090–4105, doi:10.1002/2013JB010641.

Shibazaki, B., and T. Shimamoto (2007), Modelling of short-interval silent slip events in deeper subduction interfaces considering the frictional properties at the unstable-stable transition regime, *Geophys. J. Int.*, *171*, 191–205, doi:10.1111/j.1365-246X.2007.03434.x.
Shimamoto, T., and J. M. Logan (1981), Effects of simulated clay gouges on the sliding behavior of Tennessee sandstone, *Tectonophysics*, *75*, 243–255.
Sibson, R. H. (1977), Fault rocks and fault mechanisms, *J. Geol. Soc. London*, *133*, 191–213.
Skarbek, R. M., A. W. Rempel, and D. A. Schmidt (2012), Geologic heterogeneity can produce aseismic slip transients, *Geophys. Res. Lett.*, *39*, L21306, doi:10.1029/2012GL053762.
Sleep, N. H. (2005), Physical basis of evolution laws for rate and state friction, *Geochem. Geophys. Geosyst.*, *6*, Q11008, doi:10.1029/2005GC000991.
Sleep, N. H. (2006), Real contacts and evolution laws for rate and state friction, *Geochem. Geophys. Geosyst.*, *7*, Q08012, doi:10.1029/2005GC001187.
Sone, H., T. Shimamoto, and D. E. Moore (2012), Frictional properties of saponite-rich gouge from a serpentinite-bearing fault zone along the Gokasho-Arashima tectonic line, central Japan, *J. Struct. Geol.*, *38*, 172–182, doi:10.1016/j.jsg.2011.09.007.
Sposito, G., N. T. Skipper, R. Sutton, S.-H. Park, A. K. Soper, and J. A. Greathouse (1999), Surface geochemistry of clay minerals, *Proc. Natl. Acad. Sci. U. S. A.*, *96*, 3358–3364, doi:10.1073/pnas.96.7.3358.
Stesky, R. M. (1978), Rock friction-effect of confining pressure, temperature, and pore pressure, *Pure Appl. Geophys.*, *116*, 690–704.
Taylor, E. W. (1949), Correlation of the Moh's hardness scale with the Vickers's hardness numbers, *Min. Mag.*, *28*, 718–721.
Tenthorey, E., and S. F. Cox (2006), Cohesive strengthening of fault zones during the interseismic period: An experimental study, *J. Geophys. Res.*, *111*, B09202, doi:10.1029/2005JB004122.
Towe, K. M. (1962), Clay mineral diagenesis as a possible source of silica cement in sedimentary rocks, *J. Sediment. Petrol.*, *32*, 26–28.
Tse, S. T., and J. R. Rice (1986), Crustal earthquake instability in relation to the depth variation of frictional slip properties. *J. Geophys. Res.*, *91*, 9452–9472.
Tullis, T. E. (1988), Rock friction constitutive behavior from laboratory experiments and its implications for an earthquake prediction field monitoring program, *Pure Appl. Geophys.*, *126*, 555–588.
Tullis, T. E., and J. D. Weeks (1986), Constitutive behavior and stability of frictional sliding of granite, *Pure Appl. Geophys.*, *124*, 383–414.
van de Kamp, P. C. (2008), Smectite-illite-muscovite transformations, quartz dissolution, and silica release in shales, *Clays Clay Miner.*, *56*, 66–81.
Van Diggelen, E. W. E., J. H. P. De Bresser, C. J. Peach and C. J. Spiers (2009), High shear strain behaviour of synthetic muscovite fault gouges under hydrothermal conditions, *J. Struct. Geol.*, *32*, 1685–1700.
Wang, W., and C. H. Scholz (1994), Micromechanics of the velocity and normal stress dependence of rock friction, *Pure Appl. Geophys.*, *143*, 303–315.
Wawersik, W. R., and D. H. Zeuch (1986), Modeling and mechanistic interpretation of creep of rock salt below 200°C, *Tectonophysics*, *121*, 125–152.
Weeks, J. D., and T. E. Tullis (1985), Frictional sliding of dolomite: A variation in constitutive behavior, *J. Geophys. Res.*, *90*, 7821–7826.
Westbrook, J. H. (1958), Temperature dependence of strength and brittleness of some quartz structures, *J. Am. Ceram. Soc.*, *41*, 433–440.
Woodcock, N. H., and K. Mort (2008), Classification of fault breccias and related fault rocks, *Geol. Mag.*, *145*, 435–440.
Zhang, G., Z. Wei, and R. E. Ferrell (2009), Elastic modulus and hardness of muscovite and rectorite determined by nanoindentation, *Appl. Clay Sci.*, *43*, 271–281, doi:10.1016/j.clay.2008.08.010.
Zhang, X., and C. J. Spiers (2005), Compaction of granular calcite by pressure solution at room temperature and effects of pore fluid chemistry, *Int. J. Rock Mech. Min. Sci.*, *42*, 950–960.